processes

MDPI

Article

A Model and Data Hybrid-Driven Method for Operational Reliability Evaluation of Power Systems Considering Endogenous Uncertainty

Lingzi Zhu [1], Qihui Chen [2], Mingshun Liu [1,*], Lingxiao Zhang [2] and Dongxu Chang [3]

[1] Power Dispatching Control Center of Guizhou Power Grid Co., Ltd., Guiyang 550008, China
[2] State Key Laboratory of Power Transmission Equipment Technology, School of Electrical Engineering, Chongqing University, Chongqing 400044, China; zhanglingxiao54@163.com (L.Z.)
[3] Electric Power Research Institute, China Southern Power Grid, Guangzhou 510663, China; changdx@csg.cn
* Correspondence: lms2800@126.com; Tel.: +86-13515016347

Abstract: Renewable energy sources are increasingly integrated into power systems, leading to significant variability in operations. This necessitates robust methods for assessing operational reliability. We propose a novel model–data hybrid approach that incorporates endogenous uncertainty into the reliability evaluation process. First, unlike traditional methods that treat uncertainties as external factors, this approach recognizes that operational decisions can significantly influence how uncertainties are resolved and impact reliability metrics. The proposed method integrates device reliability indices with operational decision variables. This allows us to evaluate the impact of endogenous uncertainty on operational reliability through a reliability-constrained stochastic unit commitment model. Additionally, a model–data hybrid algorithm is introduced for efficient solution of the formulated optimization problem. Case studies demonstrate the effectiveness of the proposed method. Results also show that endogenous uncertainty may cause a 10% error in power system reliability indices.

Keywords: operational reliability evaluation; endogenous uncertainty; power system; data-driven

Citation: Zhu, L.; Chen, Q.; Liu, M.; Zhang, L.; Chang, D. A Model and Data Hybrid-Driven Method for Operational Reliability Evaluation of Power Systems Considering Endogenous Uncertainty. *Processes* **2024**, *12*, 1056. https://doi.org/10.3390/pr12061056

Academic Editors: Chang-Hua Lin, Shiue-Der Lu and Hwa-Dong Liu

Received: 2 April 2024
Revised: 9 May 2024
Accepted: 15 May 2024
Published: 22 May 2024

1. Introduction

Modern power systems rely heavily on their reliability, which ensures the secure and adequate provision of electrical energy. Conventional power system reliability evaluations utilized historical data and assumed static failure rates for equipment like generators and transmission lines. However, recent research has highlighted the temporal variability of device performance within operational timeframes [1]. This necessitates a shift towards operational reliability evaluations that address short-term reliability under dynamic conditions, a trend that has gained significant traction in recent decades [2].

Modern power system research prioritizes operational reliability, making it a key area of focus in both academia and industry. To account for the dynamic nature of device failures, researchers have explored probabilistic reliability indicators at specific points in time (e.g., [3,4]). Additionally, studies have investigated how demand response programs influence the short-term reliability of wind-integrated power systems (e.g., [5]).

The growing complexities within power systems necessitate a closer link between operational optimization and reliability evaluation. This recognition has led to the incorporation of operational reliability metrics as either objectives or constraints in key decision-making problems. These problems include unit commitment (UC) [6,7], economic dispatch [8], reserve optimization [9], and power market clearing [10].

Previous studies primarily focused on exogenous uncertainties as the main factors influencing reliability metrics. These uncertainties include demand and renewable energy variations, as well as random equipment failures. Exogenous uncertainties are typically

assumed to have predetermined and fixed probability distributions independent of decision-making processes [1]. However, this approach overlooks the crucial role of endogenous uncertainties (EUs) in operational reliability.

EUs represent uncertainties that are influenced by operational optimization decisions, either explicitly or implicitly, and play a significant role in operational reliability evaluations. Mounting evidence suggests that operating conditions significantly impact the uncertainties associated with device states [11]. Since operational decisions directly determine these operating conditions, they also influence the resolution of uncertainties related to device states, as illustrated in Figure 1. Figure 1 demonstrates how decision variables determine the operating conditions of generation and transmission equipment, which further affect the devices' force outage rates (FORs). Consequently, uncertainties related to device states emerge as a key example of EUs.

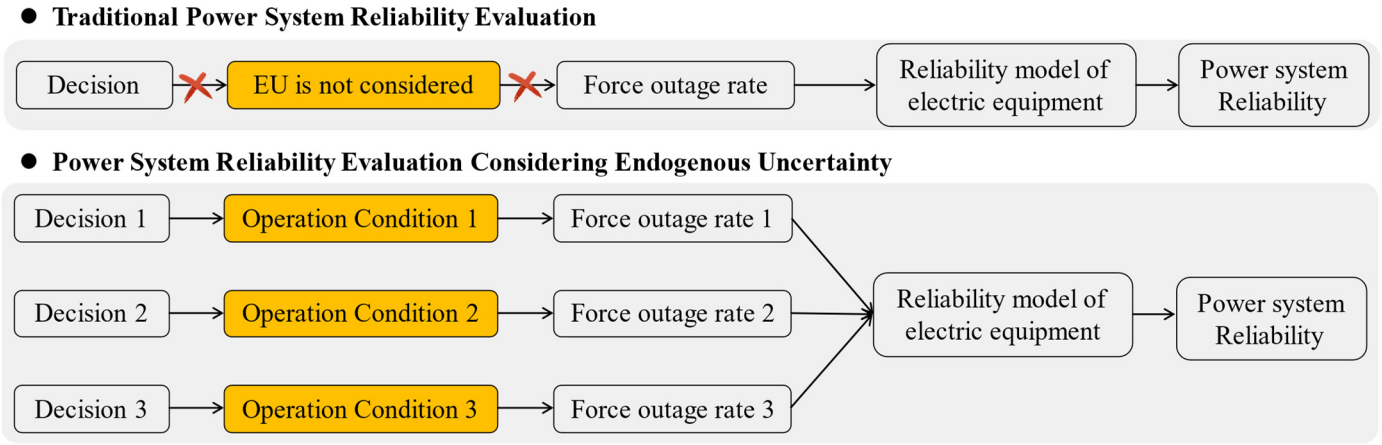

Figure 1. Comparisons between the conventional power system reliability evaluation and the one considering endogenous uncertainty.

The presence of EUs exerts a substantial impact on operational reliability, necessitating a comprehensive approach that considers both optimization and evaluation as an interconnected process. By incorporating EUs into our understanding of operational reliability, we can achieve more accurate and robust decision making, ultimately enhancing the security and efficiency of power systems.

Traditionally, evaluating power system reliability is a time-consuming process. This is because optimal power flow (OPF) calculations are performed on an exponentially growing number of system states to determine load shedding for each state. To address this complexity, the direct current (DC) model is often used as a computationally simpler alternative to the full AC model. However, even with this simplification, reliability evaluation for a provincial system can still take several to dozens of hours. The inclusion of endogenous uncertainty further exacerbates this issue by dramatically increasing the number of possible system states, making the evaluation even more computationally expensive. Additionally, system fluctuations caused by renewable energy sources lead to dynamic changes in reliability over time. This dynamic nature makes it challenging to ensure timely assessments of operational reliability. As a result, developing methods for faster and more efficient reliability evaluation becomes increasingly crucial.

Several approaches have been proposed to address the computational challenges associated with operational reliability evaluation. Techniques like fast sorting algorithms [12], state-space decomposition [13,14], and dimensionality reduction [15,16] have been developed to minimize the number of states considered. Similarly, reliability evaluation using Monte Carlo simulation (MCS) [17] has seen advancements through state space pruning [18], population-based intelligent search [19], and advanced sampling techniques like Latin hypercube sampling [20,21]. These methods primarily focus on accelerating the simulation process by reducing the number of system states explored.

However, a separate set of techniques aims to expedite the analysis of individual system states. These methods, such as the Lagrange multiplier-based state enumeration (LMSE) [22], the multiparametric linear program (MPLP) [23,24], and the load feasible region (LFR) approach [25], bypass the need for full optimal power flow (OPF) calculations for each state by employing alternative methods to determine load shedding requirements. While existing methods offer faster reliability evaluation through reduced state exploration and analysis, they struggle to keep pace with the dynamic nature of renewable energy. Any fluctuation necessitates a full re-evaluation, hindering real-time insights. To address this timeliness issue, a new approach is needed: a rolling reliability assessment that utilizes real-time data. This method would continuously update the evaluation, eliminating the need for repetitive full assessments.

Current methods for operational reliability evaluation have limitations. This paper addresses these shortcomings by introducing a new approach. The key contributions of this article are as follows:

(1) Propose an explicit and analytical EU model to reveal the relationship between operational decisions and the power components' reliability parameters.
(2) Develop a model and data hybrid-driven method to evaluate the transmission system reliability considering EUs. An M-BPNN architecture is employed for faster and potentially more accurate assessments. The M-BPNN is trained offline using a non-sequential Monte Carlo simulation to calculate system reliability indices under various operating conditions. Following this training, the system states are categorized, and separate BP neural networks are trained specifically for each category. During online operation, real-time system data are fed into the corresponding pre-trained neural network to obtain reliability metrics.

The remainder of this paper is organized as follows. Section 2 presents the model of endogenous uncertainty in power systems. Section 3 introduces the power system reliability evaluation model considering the endogenous. Section 4 proposes the model and data hybrid-driven reliability evaluation method. Numerical results are given in Section 5. Section 6 concludes this manuscript.

2. Modeling of EU in Power Systems

2.1. Concept of EU

To delve into the concept of the EU, it is crucial to establish a clear distinction between it and its counterpart, exogenous uncertainty. Exogenous uncertainty refers to situations with inherent and substantial uncertainties. In such cases, the underlying probability distribution of stochastic parameters can be established based on historical data or expert knowledge. Conversely, the EU arises when decisions made at a specific point in time significantly impact the level of uncertainty encountered later.

Within the realm of the EU, two primary model categories exist:

- Type I: Decisions can shift the probability distribution of uncertain parameters, making some outcomes more probable and others less [26].
- Type II: Through strategic actions, the decision maker can exert control over the existing uncertainty [27].

This research delves into the complexities of a specific type of EU model (Type I). While the EU has gained traction in power system expansion planning, as evidenced by a multistage stochastic optimization model for large-scale wind [26], its application in operational reliability assessment remains less studied. Existing works like [27] explore the EU's role in investment planning for solar and concentrating solar plants. However, a comprehensive understanding of the EU's impact on operational reliability evaluation is lacking. Ignoring these multifaceted influences can lead to overly optimistic or pessimistic assessments, potentially misleading decision making in power system operations and leading to suboptimal outcomes.

2.2. EU Modeling in Power System Operational Reliability Evaluation

EU is modeled by the relationship between decision variables and electrical equipment FORs. The lifespan of equipment generally decreases with increasing operating temperature and reaction rates. Components subjected to continuous high temperatures experience a reduction in lifespan and a corresponding rise in failure probability. This is primarily because increased current flow through a component often leads to a rise in its temperature. The condition-dependent forced outage rate (FOR) of an electric component can be expressed as [28]

$$F(I) = \begin{cases} \alpha \cdot e^{\beta I}, & I_0 < I < I_1 \\ \hat{F}, & I \le I_0. \end{cases}, \tag{1}$$

where $F(I)$ is the FOR of the electric equipment, I is the real-time current, I_0 is the rated current of the equipment, and I_1 is the trip setting current. The parameter F_0 is the initial value of the FOR of the electric equipment when the current is smaller than I_0 such that [29]

$$F_0 = \frac{\lambda}{\lambda + \mu}, \tag{2}$$

where λ is the failure rate and μ is the repair rate of the electric equipment, which are set based on the historical data. Parameters α and β are calculated based on historical data such that

$$\alpha = \frac{F_0}{e^{\beta \cdot I_0}}, \tag{3}$$

$$\beta = \frac{\ln\left(\frac{F_0}{F_{\max}}\right)}{I_0 - I_1}. \tag{4}$$

The actual value of the current I can be obtained through the optimal power flow calculation. Note that the optimal power flow depends on the operational decisions of the power system, e.g., the decisions of the unit commitment. Thus, the EEU-based FOR of the ith electric equipment, denoted as F_i^{EU}, can be equivalently expressed as

$$F_i^{\mathrm{EU}} = F_i^{\mathrm{EU}}(I_i) = F_i^{\mathrm{EU}}(Q(x, y)) \tag{5}$$

$$I_i = Q(x, y) \tag{6}$$

where x is a binary variable and it represents the UC solution. y is the continuous variable and it is related to the generation schedule, etc. $Q(\cdot)$ denotes the function between the binary variable x and the continuous variable y.

Device FORs are further impacted by external uncertainties beyond inherent design limitations. These uncertainties include factors like age-related failures. Therefore, both EU and aging effects are incorporated into the reliability models for these devices. Suppose that an electric equipment has an enlistment age of t_0. Then, its FOR, denoted as $F_a^0(t_0, i)$, during the ith period is estimated as

$$F_a^0(t_0, i) = \frac{\int_{t_0}^{t_0 + i\Delta t} H(t)dt - \int_{t_0}^{t_0 + (i-1)\Delta t} H(t)dt}{\int_{t_0}^{\infty} H(t)dt}, \tag{7}$$

where $H(t)$ characterizes the likelihood of ageing-related failure as a function of time t.

There might be a dependency between outages caused by EU issues and those caused by aging equipment. Devices with longer operating lifetimes (enlistment ages) tend to be more sensitive to operational variations, increasing their susceptibility to issues arising

from endogenous uncertainties. Consequently, Equation (1) can be reformulated into a more general form as shown below.

$$F(I, T_1, i) = \begin{cases} \alpha_{\text{age}} \cdot e^{\beta_{\text{age}} \cdot I}, & I_0 < I < I_1, \\ F_a^0(t_0, i), & I \leq I_0. \end{cases} \tag{8}$$

where parameters α_{age} and β_{age} are updated by (3) and (4).

3. The EU-Guided Operational Reliability Evaluation Model

Section 3 introduces the operational reliability evaluation model for power systems considering endogenous uncertainty (EU). The operational reliability evaluation process contains three parts: (1) EU-based scenario generation; (2) stochastic unit commitment (SUC)-based system state analysis; and (3) reliability index calculations. Figure 2 shows the operational reliability evaluation process.

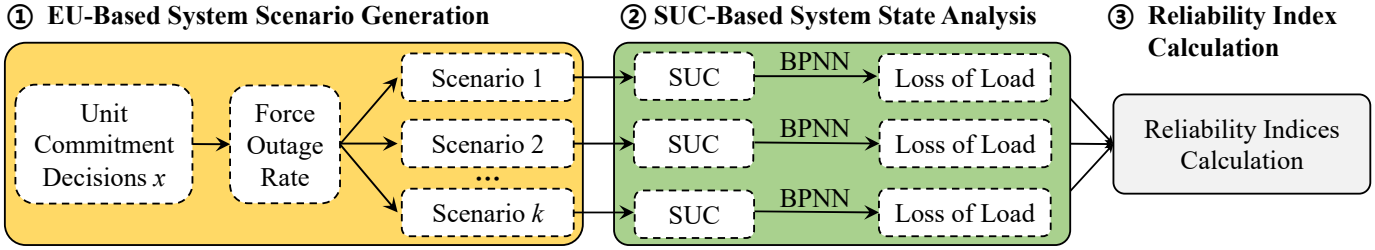

Figure 2. EU-based power system operational reliability evaluation.

3.1. EU-Based Scenario Generation

Let $\Phi_{s,\text{up}}$ be the set of available devices and $\Phi_{s,\text{dn}}$ is the set of unavailable devices corresponding to scenario s. The occurrence probabilities of scenario s can be expressed as

$$\pi_s = \left(\prod_{i \in \Phi_{s,\text{up}}} (1 - F(I, T_1, i)) \right) \cdot \left(\prod_{i \in \Phi_{s,\text{dn}}} F(I, T_1, i) \right), \tag{9}$$

where $F(I, T_1, i)$ denotes the failure rate of the ith electric component.

It is clear from (9) that the ith electric component's failure rate $F(I, T_1, i)$ is a function of the current I and the service time T_1. In contrast, the component's failure rate is modeled as a constant in conventional research [R1]–[R3] because the previous research does not consider the endogenous uncertainty.

Operational reliability evaluation often employs scenario generation techniques based on $N - k$ contingencies, where N represents the total number of system components and k represents the number of allowed simultaneous failures. Increasing the value of k leads to a more comprehensive assessment by incorporating the effects of multiple component outages. However, this approach faces a trade-off between accuracy and computational burden. As k grows the number of potential contingencies rises exponentially, significantly increasing the computational complexity required for analysis. This paper employs the Markov chain Monte Carlo method to generate system scenarios.

3.2. SUC-Based System State Analysis

The power system state analysis aims to calculate the demand curtailment under different scenarios. A two-stage SUC model is employed for system state analysis. The first stage of the SUC model determines the unit commitment variables $u_{g,t}$ and the second stage determines the dispatch variables $P_{g,t}^{\text{s}}$ after the uncertain parameter realizations. The objective function, f_g, can be expressed as the sum of the first-stage cost function $f_g^{(1)}\left(u_{g,t-1}, u_{g,t}\right)$, the second-stage cost function $f_g^{(2)}\left(P_{g,t}^{\text{s}}\right)$, and the cost of demand cur-

tailment $c_{\text{cur}} \cdot \sum_n P^{\text{s}}_{\text{cur},n,t}$, where c_{cur} is the cost coefficient of demand curtailment and $\sum_n P^{\text{s}}_{\text{cur},n,t}$ is the total demand curtailment. The objective function can be expressed as

$$\min \sum_{g\in G} \sum_{t\in T} \sum_{s\in S} \pi_s \left(f_g^{(1)}\left(u_{g,t-1}, u_{g,t}\right) + f_g^{(2)}\left(P^s_{g,t}\right) + c_{\text{cur}} \cdot \sum_n P^{\text{s}}_{\text{cur},n,t} \right). \tag{10}$$

The first-stage cost function $f_g^{(1)}\left(u_{g,t-1}, u_{g,t}\right)$ can be expressed as the sum of the startup cost of generation units, $C^{\text{U}}_{g,t}$, and the shutdown cost $C^{\text{D}}_{g,t}$:

$$f_g^{(1)}\left(u_{g,t-1}, u_{g,t}\right) = C^{\text{U}}_{g,t} + C^{\text{D}}_{g,t}. \tag{11}$$

The second-stage cost function is the operational cost of generation units such that

$$f_g^{(2)}\left(P^{\text{s}}_{g,t}\right) = c_g P^{\text{s}}_{g,t}, \tag{12}$$

where c_g is the operating cost coefficient of the gth-generation unit.

The first stage of the model incorporates constraints on unit commitment decisions $u_{g,t}$. Equations (13) and (14) ensure that each generating unit g respects minimum down-time (T_{O}) and minimum up-time (T_{S}) requirements.

$$\sum_{k=t}^{t+T_{\text{O}}-1} u_{g,k} \geq T_{\text{O}} \cdot \left(u_{g,t} - u_{g,t-1}\right) \tag{13}$$

$$\sum_{k=t}^{t+T_{\text{S}}-1} \left(1 - u_{g,k}\right) \geq T_{\text{S}} \cdot \left(u_{g,t-1} - u_{g,t}\right) \tag{14}$$

Constraints (15) and (16) address the costs associated with unit startup and shutdown, where H_g and J_g are the startup and shutdown cost coefficients for the gth-generation unit.

$$C^{U}_{g,t} \geq max\left\{H_g \cdot \left(u_{g,t} - u_{g,t-1}\right), 0\right\} \tag{15}$$

$$C^{D}_{g,t} \geq max\left\{J_g \cdot \left(u_{g,t-1} - u_{g,t}\right), 0\right\} \tag{16}$$

The second-stage incorporates various constraints, denoted by Equations (17) to (26). Equation (17) enforces power balance at each bus, considering connections with generators (represented by matrix C_g) and lines (represented by matrix C_{ft}). $P^{\text{s}}_{d,n,t}$ and $P^{\text{s}}_{\text{cur},n,t}$ represent demand and corresponding curtailment for each bus at period t.

$$C_g \cdot P^{\text{s}}_{g,t} - C_{ft} \cdot P^{\text{s}}_{l,t} = P^{\text{s}}_{d,n,t} - P^{\text{s}}_{\text{cur},n,t}. \tag{17}$$

Equation (18) governs power flow through lines, with $\Delta\theta^{\text{s}}_{l,t}$ being the voltage phase angle difference between connected buses for line l at time t.

$$P^s_{l,t} = \frac{\Delta\theta^s_{l,t}}{X_l}. \tag{18}$$

Constraint (19) ensures line power flow remains within limits, where z^{s}_l reflects the availability of line l in scenario s, and Ω_l represents the set of all lines.

$$P^{min}_l \cdot z^s_l \leq P^s_{l,t} \leq P^{max}_l \cdot z^s_l, \;\; z^s_l \in \{0,1\}. \tag{19}$$

Similarly, Constraint (20) guarantees generator outputs stay within limits, with z^{s}_g indicating the availability of unit g in scenario s, and Ω_g representing the set of all units.

$$P^{min}_g \cdot z^s_g \cdot u_{g,t} \leq P^s_{g,t} \leq P^{max}_g \cdot z^s_g \cdot u_{g,t}, \;\; z^s_g \in \{0,1\}. \tag{20}$$

Constraints (21) and (22) address ramping capabilities, limiting both upward and downward adjustments in power output. $R_{g,\mathrm{u}}$ and $R_{g,\mathrm{d}}$ represent the limits for ramping up and down, respectively. Additionally, $ST_{g,u}$ and $SD_{g,\mathrm{d}}$ denote limitations on start-up and shutdown power, respectively.

$$P^s_{g,t} - P^s_{g,t-1} \leq u_{g,t-1} \cdot \left(R_{g,u} - ST_{g,u}\right) + ST_{g,u}. \tag{21}$$

$$P^s_{g,t-1} - P^s_{g,t} \leq u_{g,t} \cdot \left(R_{g,d} - SD_{g,\mathrm{d}}\right) + SD_{g,d}. \tag{22}$$

Constraint (23) restricts the extent of demand curtailment, while Constraint (24) sets boundaries for phase angles. The availability state set for all elements is denoted by Z_s, and individual element availabilities (generators z^s_g and lines z^s_l) are members of this set Z_{s}.

$$0 \leq P^s_{\mathrm{cur},t} \leq P^{\max}_{\mathrm{cur},t}, \tag{23}$$

$$\theta^{\min} \leq \theta^s_t \leq \theta^{\max}. \tag{24}$$

Finally, Equations (25) and (26) introduce reliability-specific constraints.

$$EENS_t = \sum_n \sum_s \pi_s \cdot P^{\mathrm{s}}_{\mathrm{cur},n,t}, \tag{25}$$

$$EENS_t \leq \overline{EENS}, \tag{26}$$

where $\overline{EENS}$ are the maximum value of $EENS_t$. Definition of $EENS_t$ is given in Section 3.3.

3.3. Reliability Index Calculations

The reliability metrics used to quantify operational reliability include the expected energy not supplied (EENS) and loss of load probability (LOLP). EENS refers to the amount of electricity demand that is anticipated to go unmet within a specific timeframe such that

$$EENS_t = \Delta t \cdot \sum_s \pi_s \cdot P^s_{cur,t}, \tag{27}$$

where Δt denotes the length of t that demand reduction occurs. $P^{\mathrm{s}}_{\mathrm{cur},t}$ denotes the demand curtailment in period t corresponding to scenario s.

LOLP measures the likelihood that the electrical system will not be able to meet the demand for electricity within a year such that

$$LOLP_t = \sum_s \pi_{s,t} \cdot L_{s,t}, \tag{28}$$

where $L_{s,t}$ is a binary variable and it is equal to 1 if the demand curtailment happens in scenario s, it is equal to 0 otherwise; that is,

$$L_{s,t} = \begin{cases} 0, & P^s_{cur,t} \leq 0, \\ 1, & P^s_{cur,t} > 0. \end{cases} \tag{29}$$

4. The Model and Data-Driven Algorithm

Evaluating operational reliability in power systems is a complex task due to the sheer size and interconnectedness of modern grids. Traditional methods, such as $N-k$ contingency analysis, become computationally expensive for large systems as they require simulating numerous outage scenarios. Backpropagation Neural Networks (BPNNs) offer a promising alternative by reducing the computational burden associated with reliability evaluation.

4.1. The Framework of BPNN

BPNNs achieve this by learning from pre-computed data. Instead of re-simulating outages every time an evaluation is needed, BPNNs can be trained on a large dataset

of pre-computed reliability assessments for various scenarios. This pre-training allows BPNNs to evaluate new operating conditions much faster than traditional methods. Additionally, the BPNN can handle uncertainties inherent in power systems. Fluctuations in renewable energy output, unpredictable load profiles, random equipment failures, and EU all contribute to the challenge of assessing reliability. BPNNs excel at learning complex relationships between these uncertain factors and their impact on the system's reliability.

A BPNN is organized into layers of interconnected artificial neurons. These layers include input layer, hidden layers, and output layer, as shown in Figure 3.

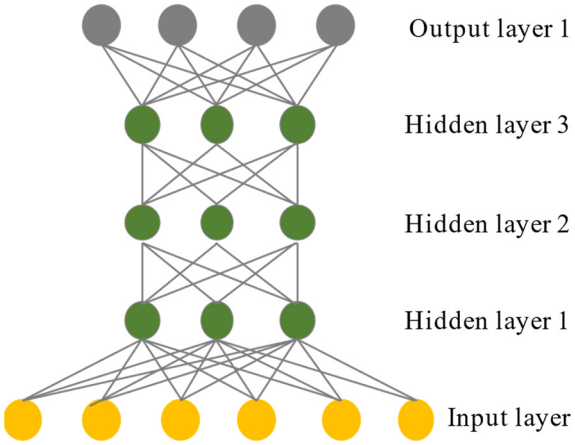

Figure 3. The structure diagram of BPNN.

The input layer receives raw data representing the state of the power system for reliability evaluation. Examples of such data include power generation, electricity demand at various grid points, and the operational status of components.

The hidden layers perform the core information processing. A BPNN can have one or more hidden layers, each containing multiple interconnected neurons. These neurons apply mathematical functions to transform the received data. The number of hidden layers and neurons significantly impacts the BPNN's ability to learn intricate relationships within the data.

The output layer produces the network's prediction or output. In the context of reliability evaluation, this output could be a single value representing the probability of a system failure or a set of values indicating the reliability of different grid components.

During forward propagation, the activation of a hidden neuron is calculated as

$$y_j = f_J(\mu_j + \omega_j y_m), \tag{30}$$

where the input layer takes in data denoted by y_m. The jth hidden layer receives its input from the previous layer, represented by y_j. Weights connecting the previous layer to neurons in the jth hidden layer are denoted by ω_j. Each neuron in the jth hidden layer has a threshold value, μ_j. The activation function applied to each neuron in the jth hidden layer is denoted by f_j.

The relationship between the hidden layer and the next hidden layer can be expressed as

$$y_{j+1} = f_J(\mu_{j+1} + \omega_{j+1} y_j). \tag{31}$$

The relationship between hidden layer and output layer can be expressed as

$$y_t = f_o(u_o + \omega_o y_{j,max}), \tag{32}$$

The model predicts a value (y_t) for each time point (t). This prediction is influenced by the weights (ω_o) connecting the final hidden layer to the output layer. Additionally, a threshold value (u_o) is applied at the output layer. The output layer utilizes an acti-

vation function (f_o) to transform the weighted sum of inputs. Commonly, hidden layer activation functions are logical or hyperbolic, while the output layer often employs a linear activation function.

To assess the model's accuracy, we can calculate the error between predicted and actual outputs using the following formula:

$$\delta_y = y_t - y, \tag{33}$$

The formula allows us to calculate the error term for a unit in the jth hidden layer as:

$$\delta_j = \omega_j^T \delta_{j+1} \times \left(f_J^* (1 - f_J) \right) \tag{34}$$

In the formula, the weight coefficient of the hidden layer j can be updated as:

$$\omega_j = \omega_j + \delta_{j+1} \cdot y_j^T \tag{35}$$

This describes one iteration of training a Multi-Backpropagation Neural Network (M-BPNN). Through repeated adjustments of its learning parameters over numerous iterations, the M-BPNN progressively refines its accuracy.

4.2. BPNN Based Operational Reliability Evaluation Algorithm

This work introduces a novel approach, the Multi-Backpropagation Neural Network (M-BPNN) architecture, to improve the prediction accuracy of system reliability indices under fluctuating operating conditions. Conventional BPNN models directly map operating conditions to reliability metrics. However, the impact of different operating points on reliability varies as conditions change. This limitation can lead to inaccurate predictions with a single BPNN architecture.

The proposed M-BPNN addresses this limitation by introducing a classification step before network training. The system operating data are first categorized based on a chosen attribute, such as mean or quantile values. This allows for the creation of multiple BPNN sub-models, each trained on data with similar characteristics. During prediction, the input data from the test set are first classified and then directed to the corresponding sub-model for prediction. Finally, the results from all sub-models are combined to form the complete forecast.

The effectiveness of BPNNs is significantly influenced by the number of hidden layers and neurons within these layers. To address this, the paper proposes an adaptive algorithm for finding the optimal architecture for the M-BPNN. This algorithm iteratively evaluates different network configurations and selects the one that delivers the most accurate prediction results. It contains eight steps.

Step 1. Input Data: The process starts with feeding the training and test datasets to the system.
Step 2. Set Maximum Values: The network architecture has a predetermined maximum number of hidden layers and units per layer.
Step 3. Enumeration: The flowchart utilizes a cyclical process to iteratively assess various configurations of hidden layers and the number of elements within those layers, all while staying within predefined limits.
Step 4. BPNN Training: The loop iteratively trains a Backpropagation Neural Network with the chosen configuration of hidden layers and elements.
Step 5. Error Calculation: After training the network, the BP neural network is used to calculate the reliability index and the error.
Step 6. Termination Condition: The loop iterates until all possible combinations of hidden layers and hidden elements have been enumerated.
Step 7. Minimum Error Selection: Once all combinations are assessed, the flowchart finds the combination that resulted in the minimum error.

Step 8. Reliability Index Calculation: Finally, the flowchart employs the identified combination of hidden layers and hidden elements to calculate the reliability index.

5. Numerical Results

Case studies were carried out with numerical experiments to examine the benefits of the proposed method in the efficiency improvement of power system operational reliability evaluation. Five power system reliability evaluation methods are considered.

- Method 1 (M1): The non-sequential Monte Carlo simulation method. The convergence threshold of the sequential Monte Carlo method is 10^{-4}.
- Method 2 (M2): The proposed method.
- Method 3 (M3): The radial basis function (RBF) neural network-based method [30]. The RBF neural network also has an input layer, hidden layer, and output layer. The RBF neural network is trained using a supervised learning algorithm such as gradient descent or its variants. During training, the network adjusts the weights associated with the radial basis functions and the output layer to minimize the difference between the predicted reliability values and the actual reliability data (obtained from historical records, simulations, or analytical models). A detailed structure can be found in [30].
- Method 4 (M4): The generalized regression neural network-based method [31]. The generalized regression neural network has the input layer, the radial basis layer, and the output layer. The radial basis layer calculates the Euclidean distance between the input vector and each prototype vector. The distance calculation is typically performed using a Gaussian kernel function. The outputs from the radial basis layer are weighted by the Gaussian activations and summed to produce the final output of the network. Details can be found in [31].
- Method 5 (M5): The genetic algorithm [32]. The genetic algorithm contains eight parts: (1) chromosome representation, (2) initialization, (3) fitness evaluation, (4) selection, (5) crossover, (6) mutation, (7) replacement, and (8) termination. Details can be found in [32].

Three test systems are considered, including the RTS 79 system, the RBTS system, and the RTS 96 system. The data source and the diagram of these test systems can be found in [2] The evaluation process commences with the calculation of system reliability indices under various operating conditions using M1. These calculated indices subsequently serve as both the input and output data for methods M2–M4. Next, the data are divided into training and test sets following a 9:1 ratio. The training set is used to train the neural network model, while the test set serves the purpose of verifying the model's accuracy. This process can avoid overfitting.

Consider the results of the unit commitment of the RBTS system as an example. The RBTS system comprises six buses, nine transmission lines, and a mix of generation units including four thermal and seven hydro units. It caters to five demand centers with a total installed generation capacity of 240 MW, exceeding the peak demand of 185 MW. Daily demand curves from the IEEE- RBTS inform the demand models. For manageability, the maximum number of simultaneously failing devices is limited to three. The capacity and reliability parameters of the system components are detailed in Table 1. The analysis considers a total of 1351 scenarios encompassing all possible "N-3" contingencies. For reference, a comprehensive list of "N-1," partial "N-2," and "N-3" scenarios is provided in Table 2.

Table 1. Reliability Parameters of the Electric Equipment of the RBTS System.

Electric Equipment	Rated Capacity (MW)	Failure Rate (occ./a)	Repair Rate (occ./a)	Force
The 1st generator	40	2.0	194.67	0.0300
The 2nd generator	40	2.0	194.67	0.0300
The 3rd generator	10	4	194.67	0.0200
The 4th generator	20	2.4	159.27	0.0250
The 5th generator	5	2.4	159.27	0.0100
The 6th generator	5	2.4	159.27	0.0100
The 7th generator	40	2.4	159.27	0.0200
The 8th generator	20	5.0	194.67	0.0150
The 9th generator	20	3.0	146.00	0.0150
The 10th generator	20	6.0	194.67	0.0150
The 11th generator	20	6.0	194.67	0.0150
The 1st transmission line	45	1.5	876.00	0.0017
The 2nd transmission line	40	5.0	876.00	0.0057
The 3rd transmission line	40	4.0	876.00	0.0045
The 4th transmission line	71	1.0	876.00	0.0011
The 5th transmission line	71	1.0	876.00	0.0011
The 6th transmission line	45	1.5	876.00	0.0017
The 7th transmission line	42	5.0	876.00	0.0057
The 8th transmission line	71	1.0	876.00	0.0011
The 9th transmission line	71	1.0	876.00	0.0011

Table 2. Probability of the System Event Considering EU.

	Method		Event 1	Event 2	Event 3	Event 4	Event 5	Event 6	Event 7
N-1 system event	No EU		0.7935	0.1619	0.2035	0.2454	0.0801	0.1213	0.1213
	With EU	t_1	0.6528	0.1138	0.1430	0.1725	0.2519	0.3812	0.3812
		t_2	0.6526	0.1137	0.1429	0.1723	0.2517	0.3809	0.3809
		t_3	0.6526	0.1137	0.1428	0.1723	0.2516	0.3808	0.3808
		t_4	0.6528	0.1138	0.1429	0.1724	0.2518	0.3811	0.3811
		t_5	0.6723	0.1227	0.1542	0.1859	0.0607	0.4110	0.4110

Table 3 compares the performance of each method (M1–M5) across three test systems, including the RTS 79 system, the RBTS system, and the RTS 96 system. M1 provides the precise results while it is time-consuming. Methods M2~M5 cannot provide the optimal results but they are faster than M1. By comparing M2 with M3-M5 in each test system, we can assess the trade-off between accuracy and computational efficiency.

Table 3. Reliability Evaluation Results of Methods M1–M5.

Methods	EENS (MWh/a)			LOLP		
	RBTS System	RTS 79 System	RTS 96 System	RBTS System	RTS 79 System	RTS 96 System
M1	1056	127,549	24,704	0.0098	0.0846	0.0139
M2	1021	126,877	24,872	0.0097	0.0835	0.0138
M3	1098	124,791	22,950	0.0108	0.0909	0.0136
M4	998	147,313	20,760	0.0104	0.0917	0.0140
M5	1007	136,690	24,499	0.0090	0.0893	0.0133

The arrows in the table indicate how each method's results (EENS and LOLP) compare to the standard method (M1) within the same test system. Consider the results of the RBTS system as an example. M1 gives the baseline value of EENS as 1056 MWh/a. M2's EENS value (1021 MWh/a) is lower than M1's, indicating a closer approximation. M3's EENS value (1098 MWh/a) is higher than M1's, indicating a larger deviation. M4's EENS value (998 MWh/a) is lower than M1's, but the magnitude of the difference might be significant

compared to M2. M5's EENS value (1007 MWh/a) is lower than M1's, but the magnitude of the difference might be larger than M2's.

Figure 4 compares the absolute errors of four approximation methods (M2, M3, M4, and M5) to a standard method (M1) for evaluating the reliability of three test systems. The y-axis of the graph shows the absolute error, while the x-axis shows the evaluation method. Each method is represented by a different color line in the graph. There are two graphs in the figure, one for each metric: absolute error of EENS (equivalent energy non-supplied) and absolute error of LOLP (loss of load probability).

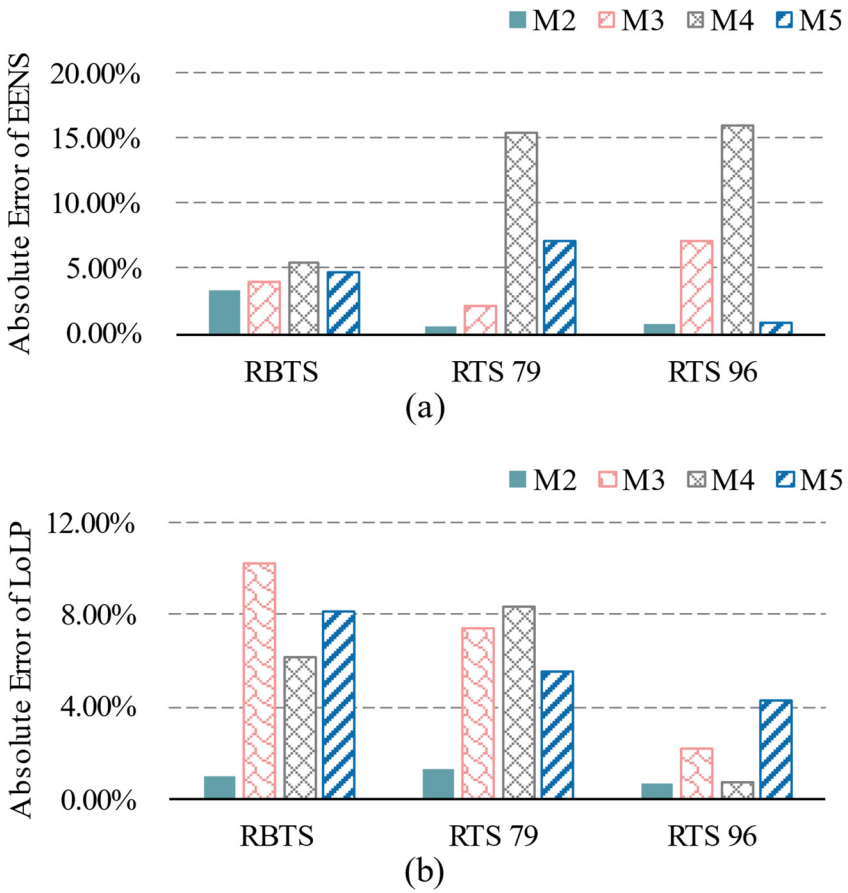

Figure 4. Absolute errors of power system reliability evaluation methods M2-M5. (**a**) Absolute errors of EENS. (**b**) Absolute errors of LOLP.

The absolute error in EENS is generally lower for method M2 compared to M3, M4, and M5 on RBTS, RTS-79, and RTS-96 systems. This suggests that M2 provides a better approximation to the standard method (M1) in terms of EENS for these systems.

The absolute error in LOLP is also lower for method M2 compared to M3, M4, and M5 on both RBTS, RTS-79, and RTS-96 systems. This suggests that M2 provides a better approximation to the standard method (M1) in terms of LOLP for these systems as well.

Overall, the graph suggests that approximation method M2 offers the closest approximation to the standard method (M1) among the four methods evaluated (M2, M3, M4, and M5) for both EENS and LOLP on the RBTS, RTS-79, and RTS-96 systems.

6. Conclusions

This paper introduces the concept of endogenous uncertainty for power system operational reliability evaluation. Endogenous uncertainty is integrated into the reliability parameter model of electric components and the scenario generation process. Then, a two-stage reliability-constrained unit commitment model is formulated for system state analysis. A BPNN-based method is proposed to solve this model. Case studies are car-

ried out on the RBTS, RTS-79, and RTS-96 systems. Numerical results demonstrate that endogenous uncertainty has a great impact on the power system reliability level. The proposed method can solve this problem more effectively compared to the radial basis function neural network-based method, the generalized regression neural network-based method, and the genetic algorithm.

Author Contributions: Methodology, L.Z. (Lingzi Zhu); Software, Q.C.; Validation, Q.C.; Formal analysis, Q.C. and D.C.; Investigation, D.C.; Resources, L.Z. (Lingzi Zhu); Data curation, L.Z. (Lingzi Zhu); Writing—original draft, M.L.; Writing—review & editing, L.Z. (Lingxiao Zhang); Visualization, L.Z. (Lingxiao Zhang); Supervision, L.Z. (Lingxiao Zhang); Project administration, D.C.; Funding acquisition, M.L. All authors have read and agreed to the published version of the manuscript.

Funding: This work was supported by the Key Science and Technology Project of China Southern Power Grid under Grant 066500KK52222013.

Data Availability Statement: The original contributions presented in the study are included in the article, further inquiries can be directed to the corresponding author.

Conflicts of Interest: Authors Lingzi Zhu and Mingshun Liu are employed by the Power Dispatching Control Center of Guizhou Power Grid Co., Ltd. Dongxu Chang are employed by the Electric Power Research Institute, China Southern Power Grid. The remaining authors declare that the research was conducted in the absence of any commercial or financial relationships that could be construed as a potential conflict of interest. The authors declare that this study received funding from China Southern Power Grid. The funder was not involved in the study design, collection, analysis, interpretation of data, the writing of this article or the decision to submit it for publication.

Nomenclature

Indices and Sets	
i	Index of power components
g	Index of generation units
t	Index of time
s	Index of scenario
$\Phi_{s,\mathrm{up}}$	Set of available devices under scenario s
$\Phi_{s,\mathrm{dn}}$	Set of unavailable devices under scenario s
Parameters	
I_0	Rated current of the power component
I_1	Trip setting current
F_0	Initial value of the forced outage rate of the electric equipment
α, β	Power outage coefficients of power components
$\alpha_{\mathrm{age}}, \beta_{\mathrm{age}}$	Power outage coefficients of power components considering aging
λ	Failure rate of the power component
μ	Repair rate of the power component
$F_{\max}$	Maximum force outage rate of the electric equipment
T_1	Service time of power component
N	The total number of power components
c_{cur}	Cost coefficient of demand curtailment
c_g	Operating cost coefficient of the gth-generation unit
T_{O}	Minimum downtime of generation units
T_{S}	Minimum up-time of generation units
H_g	Startup cost coefficients of generation units
J_g	Shutdown cost coefficients of generation units
X_l	Transmission line impedance
$P_l^{min/\max}$	Minimum and maximum transmission power of line l

$P_g^{min/\max}$	Minimum and maximum power of generation unit g
$R_{g,\mathrm{u}}$,$R_{g,\mathrm{d}}$	Limits for ramping up and down
Variables	
F	Forced outage rate of the electric equipment
I_t	Real-time current
F_i^{EU}	EU based force outage rate of the ith power component
$H(t)$	Likelihood of aging-related failure
π_s	Occurrence probability of scenario s
$u_{g,t}$	Unit commitment decision variables
$P_{g,t}^{\mathrm{s}}$	Dispatch variables
f_g	Objection function of the SUC model
$f_g^{(1)}$	First-stage cost function
$f_g^{(2)}$	Second-stage cost function
$P_{\mathrm{cur},n,t}^{\mathrm{s}}$	Demand curtailment
$C_{g,t}^{\mathrm{U}}$	Startup cost of generation units
$C_{g,t}^{\mathrm{D}}$	Shutdown cost of generation units
$P_{d,n,t}^{\mathrm{s}}$	Demand at each bus
$\Delta\theta_{l,t}^{\mathrm{s}}$	Voltage phase angle difference
z_l^s	Availability of line l in scenario s
z_g^s	Availability of generation unit g in scenario s
$ST_{g,u}$,$SD_{g,\mathrm{d}}$	Limitations on start-up and shutdown power

References

1. Pan, C.; Hu, B.; Shao, C.; Xu, L.; Xie, K.; Wang, Y.; Anvari-Moghaddam, A. Reliability-Constrained Economic Dispatch With Analytical Formulation of Operational Risk Evaluation. *IEEE Trans. Power Syst.* **2024**, *39*, 4422–4436. [CrossRef]
2. Li, X.; Xie, K.; Shao, C.; Hu, B. A Region-Based Approach for the Operational Reliability Evaluation of Power Systems with Renewable Energy Integration. *IEEE Trans. Power Syst.* **2023**, *39*, 3389–3400. [CrossRef]
3. Zhang, S.; Zhu, Z.; Li, Y. A critical review of data-driven transient stability assessment of power systems: Principles, prospects, and challenges. *Energies* **2021**, *14*, 7238. [CrossRef]
4. Liu, J.; Fan, Y.; Hou, J.; Bai, X. Reliability Evaluation of DC/DC Converter in Direct Current Collection System of Wind Farm Considering the Influence of Control Strategy. *Processes* **2023**, *11*, 2825. [CrossRef]
5. Hui, H.; Ding, Y.; Shi, Q.; Li, F.; Song, Y.; Yan, J. 5G network-based Internet of Things for demand response in smart grid: A survey on application potential. *Appl. Energy* **2020**, *257*, 113972. [CrossRef]
6. Rahmani, M.; Hosseinian, S.H.; Abedi, M. Stochastic two-stage reliability-based security-constrained unit commitment in a smart grid environment. *Sustain. Energy Grids Netw.* **2020**, *22*, 100348. [CrossRef]
7. Montero, L.; Bello, A.; Reneses, J. A review on the unit commitment problem: Approaches, techniques, and resolution methods. *Energies* **2022**, *15*, 1296. [CrossRef]
8. Lin, L.; Guan, X.; Peng, Y.; Wang, N.; Maharjan, S.; Ohtsuki, T. Deep reinforcement learning for economic dispatch of a virtual power plant in internet of energy. *IEEE Internet Things J.* **2020**, *7*, 6288–6301. [CrossRef]
9. Li, Y.; Han, M.; Yang, Z.; Li, G. Coordinating flexible demand response and renewable uncertainties for scheduling of community integrated energy systems with an electric vehicle charging station: A bi-level approach. *IEEE Trans. Sustain. Energy* **2021**, *12*, 2321–2331. [CrossRef]
10. Stoft, S. Power system economics. *J. Energy Lit.* **2002**, *8*, 94–99.
11. Sun, Y.; Wang, P.; Cheng, L.; Liu, H. Operational reliability assessment of power systems considering condition-dependent failure rate. *IET Gener. Transm. Distrib.* **2010**, *4*, 60–72. [CrossRef]
12. Liu, H.; Sun, Y.; Cheng, L.; Wang, P.; Xiao, F. Online short-term reliability evaluation using a fast sorting technique. *IET Gener. Transm. Distrib.* **2008**, *2*, 139–148. [CrossRef]
13. Bai, G.; Liu, T.; Zhang, Y.-a.; Tao, J. An improved method for reliability evaluation of two-terminal multistate networks based on state space decomposition. *IEEE Trans. Reliab.* **2020**, *70*, 1084–1095. [CrossRef]
14. Liu, T.; Bai, G.; Tao, J.; Zhang, Y.-A.; Fang, Y. An improved bounding algorithm for approximating multistate network reliability based on state-space decomposition method. *Reliab. Eng. Syst. Saf.* **2021**, *210*, 107500. [CrossRef]
15. Lin, C.; Hu, B.; Shao, C.; Ye, Y.; Tai, H.M.; Xie, K.; Jiao, D.; Li, W. Event-Triggered Load Frequency Control Based on Age-of-Information. *IEEE Trans. Power Syst.* **2022**, *38*, 2348–2361. [CrossRef]
16. Lin, C.; Hu, B.; Shao, C.; Li, W.; Li, C.; Xie, K. Delay-Dependent Optimal Load Frequency Control for Sampling Systems with Demand Response. *IEEE Trans. Power Syst.* **2022**, *37*, 4310–4324. [CrossRef]
17. Li, W. *Reliability Assessment of Electric Power Systems Using Monte Carlo Methods*; Springer Science & Business Media: Berlin/Heidelberg, Germany, 2013.

18. Andreasen, M.M.; Fernández-Villaverde, J.; Rubio-Ramírez, J.F. The pruned state-space system for non-linear DSGE models: Theory and empirical applications. *Rev. Econ. Stud.* **2018**, *85*, 1–49. [CrossRef]
19. Wang, L.; Singh, C. Population-based intelligent search in reliability evaluation of generation systems with wind power penetration. *IEEE Trans. Power Syst.* **2008**, *23*, 1336–1345. [CrossRef]
20. Shu, Z.; Jirutitijaroen, P. Latin hypercube sampling techniques for power systems reliability analysis with renewable energy sources. *IEEE Trans. Power Syst.* **2011**, *26*, 2066–2073.
21. Zhang, J.; Wang, B.; Ma, H.; Li, Y.; Yang, M.; Wang, H.; Ma, F. A Fast Reliability Evaluation Strategy for Power Systems under High Proportional Renewable Energy—A Hybrid Data-Driven Method. *Processes* **2024**, *12*, 608. [CrossRef]
22. Liu, Z.; Hou, K.; Jia, H.; Zhao, J.; Wang, D.; Mu, Y.; Zhu, L. A Lagrange multiplier based state enumeration reliability assessment for power systems with multiple types of loads and renewable generations. *IEEE Trans. Power Syst.* **2020**, *36*, 3260–3270. [CrossRef]
23. Yong, P.; Zhang, N.; Kang, C.; Xia, Q.; Lu, D. MPLP-based fast power system reliability evaluation using transmission line status dictionary. *IEEE Trans. Power Syst.* **2018**, *34*, 1630–1640. [CrossRef]
24. Zhang, J.; Wang, B.; Ma, H.; He, Y.; Wang, Y.; Xue, Z. Reliability Evaluation of Cabled Active Distribution Network Considering Multiple Devices—A Generalized MILP Model. *Processes* **2023**, *11*, 3404. [CrossRef]
25. Lin, C.; Hu, B.; Shao, C.; Niu, T.; Cheng, Q.; Li, C.; Xie, K. An analysis of delay-constrained consensus-based optimal algorithms in virtual power plants. *ISA Trans.* **2021**, *125*, 189–197. [CrossRef] [PubMed]
26. Zhan, Y.; Zheng, Q.P.; Wang, J.; Pinson, P. Generation expansion planning with large amounts of wind power via decision-dependent stochastic programming. *IEEE Trans. Power Syst.* **2016**, *32*, 3015–3026. [CrossRef]
27. Giannelos, S.; Konstantelos, I.; Strbac, G. Option value of demand-side response schemes under decision-dependent uncertainty. *IEEE Trans. Power Syst.* **2018**, *33*, 5103–5113. [CrossRef]
28. Hu, B.; Pan, C.; Shao, C.; Xie, K.; Niu, T.; Li, C.; Peng, L. Decision-Dependent Uncertainty Modeling in Power System Operational Reliability Evaluations. *IEEE Trans. Power Syst.* **2021**, *36*, 5708–5721. [CrossRef]
29. Lin, C.; Hu, B.; Shao, C.; Xie, K.; Peng, J.C.H. Computation Offloading for Cloud-Edge Collaborative Virtual Power Plant Frequency Regulation Service. *IEEE Trans. Smart Grid*, 2024; *early access*. [CrossRef]
30. Zhao, Z.-D.; Lou, Y.-Y.; Ni, J.-H.; Zhang, J. RBF-SVM and its application on reliability evaluation of electric power system communication network. In Proceedings of the 2009 International Conference on Machine Learning and Cybernetics, Baoding, China, 12–15 July 2009; pp. 1188–1193.
31. Bakkiyaraj, R.A.; Kumarappan, N. State Adequacy Evaluation Using Generalized Regression Neural Network for Non-Sequential Monte Carlo Simulation Based Composite Power System Reliability Analysis. *ICTACT J. Soft Comput.* **2012**, *3*, 408–414. [CrossRef]
32. Samaan, N.A.; Singh, C.; Levitin, G. *Reliability Assessment of Composite Power Systems Using Genetic Algorithms*; Springer: Berlin/Heidelberg, Germany, 2007.